Black carbon in aerosol during BIBLE B

J. Ben Liley,[1] D. Baumgardner,[2] Y. Kondo,[3] K. Kita,[3] D. R. Blake,[4] M. Koike,[5] T. Machida,[6] N. Takegawa,[7,8] S. Kawakami,[9] T. Shirai,[9] and T. Ogawa[9]

Received 11 May 2001; revised 24 December 2001; accepted 10 January 2002; published 14 November 2002.

[1] The Biomass Burning and Lightning Experiment (BIBLE) A and B campaigns over the tropical western Pacific during springtime deployed a Gulfstream-II aircraft with systems to measure ozone and numerous precursor species. Aerosol measuring systems included a MASP optical particle counter, a condensation nucleus (CN) counter, and an absorption spectrometer for black carbon. Aerosol volume was very low in the middle and upper troposphere during both campaigns, and during BIBLE A, there was little aerosol enhancement in the boundary layer away from urban areas. In BIBLE B, there was marked aerosol enhancement in the lowest 3 km of the atmosphere. Mixing ratios of CN in cloud-free conditions in the upper troposphere were in general higher than in the boundary layer, indicating new particle formation from gaseous precursors. High concentrations of black carbon were observed during BIBLE B, with mass loadings up to 40 $\mu g\ m^{-3}$ representing as much as one quarter of total aerosol mass. Strong correlations with hydrocarbon enhancement allow the determination of a black carbon emission ratio for the fires at that time. Expressed as elemental carbon, it is about 0.5% of carbon dioxide and 6% of carbon monoxide emissions from the same fires, comparable to methane production, and greater than that of other hydrocarbons. *INDEX TERMS:* 0305 Atmospheric Composition and Structure: Aerosols and particles (0345, 4801); 0322 Atmospheric Composition and Structure: Constituent sources and sinks; 0365 Atmospheric Composition and Structure: Troposphere—composition and chemistry; *KEYWORDS:* black carbon, biomass burning, NHMC

Citation: Liley, J. B., et al., Black carbon in aerosol during BIBLE B, *J. Geophys. Res.*, *107*, 8399, doi:10.1029/2001JD000845, 2002. [printed *108*(D3), 2003]

1. Introduction

[2] Airborne black carbon is ubiquitous in the atmosphere, where it dominates absorption of visible radiation, and as such it has a vital primary role in Earth's radiative balance. It has a secondary role through inclusion in cloud droplets, where it enhances absorption and may change cloud albedo and extent [*Ackerman et al.*, 2000]. Global production of black carbon aerosol has been estimated [*Cooke and Wilson*, 1996] at around 6 Tg from biomass burning and 8 Tg from fossil fuel combustion. Both produce soot comprising elemental or graphitic carbon, organic molecules, and a range of other chemical species. The organic species, with optical properties in a range between those of black carbon and the ubiquitous sulfate aerosol, are thought to dominate total particulate carbon emissions [*Liousse et al.*, 1996], and they may also be important in the chemical and cloud microphysical properties of soot. Elemental carbon is hydrophobic before activation by sulfuric acid [*Rawlins et al.*, 1996], but soot from combustion already incorporates water vapor and reacts with a range of chemical species [*Chughtai et al.*, 1996]. The organic carbon content of soot may provide an alternative to sulfate activation for black carbon uptake into cloud condensation nuclei, which may consist in large measure of organic aerosol [*Novakov and Penner*, 1993]. Black carbon is known to be incorporated into a large proportion of the global submicrometer aerosol burden [*Pósfai et al.*, 1999].

[3] Estimates of global black carbon aerosol depend on measurements that relate its production to that of other emissions, especially the oxides of carbon which are the major products of combustion, and to hydrocarbons which serve as tracers of biomass or other burning. Here we report such correlations from the Biomass Burning and Lightning Experiments A and B over northern Australia and Indonesia during August–September in 1998 and 1999. Biomass

[1]NIWA Lauder, Central Otago, Otago, New Zealand.
[2]UNAM, Centro de Ciencias de la Atmosfera, Ciudad Universitaria, Mexico.
[3]Research Center for Advanced Science and Technology, University of Tokyo, Japan.
[4]Department of Chemistry, University of California, Irvine, California, USA.
[5]Department of Earth and Planetary Science, University of Tokyo, Japan.
[6]National Institute for Environmental Studies, Tsukuba, Japan.
[7]Solar-Terrestrial Environment Laboratory, Nagoya University, Toyokawa, Japan.
[8]Now at Research Center for Advanced Science and Technology, University of Tokyo, Japan.
[9]Earth Observation Research Center, NASDA, Tokyo, Japan.

0148-0227/02/2001JD000845

burning activity was high over northern Australia during BIBLE B, and the Gulfstream-II sampled air masses with high concentrations of combustion tracers [*Kondo et al.*, 2002; *Shirai et al.*, 2002], especially during flights 6 (2 September 1999) and 7 (4 September 1999).

2. Aerosol Instrumentation

[4] Aerosol measurements on the Diamond Air Service Gulfstream-II (G-II) aircraft for BIBLE were obtained with three instruments: a Multiple-Angle Aerosol Spectrometer Probe (MASP), a Condensation Nucleus Counter (CNC), and a Particle Soot/Absorption Photometer (PSAP).

[5] A MASP [*Baumgardner et al.*, 1995] determines the size and concentration of particles from about 0.3 to 40 μm in diameter, and the index of refraction for particles in the diameter range 0.4 to 0.7 μm. Individual particles in the sampling air stream are detected as they transit a 780 nm laser beam. A Mangin mirror collects light scattered into the upstream hemisphere, reflecting it through condensing optics and beam splitters to four detectors. The sampling region is imaged onto the "masked aperture" detector so that the particles passing through the center of the laser beam can be distinguished for analysis, but all particles are counted. Particle size is determined from the intensity of scattered light in the "open aperture" detector, according to Mie theory. The light collected by the Mangin mirror comes mostly from two ranges of scattering angle: 30 to 60 degrees ("forward") and 120 to 150 degrees ("backward"), which are split to the respective detectors. Particle refractive index for some sizes of particles can be calculated from the ratio of forward to backward scattered light. The data acquisition system records the signal in each detector, transit time, and inter particle arrival time for each particle up to a prescribed number per second. From these data the particle size spectrum and its moments, the particle concentration, surface area, and volume, can be reconstructed in later analysis.

[6] A shrouded inlet minimizes the effect of changing angle of attack, and maintains isokinetic flow through the sensing volume to avoid concentration changes or volatilization of particles, but a MASP needs to sample where air stream disturbance by the aircraft is minimal. On the G-II, the MASP is mounted below and forward of the (port) wing tip. At normal flight speed of 200 m s^{-1}, the instrument samples ~10 cm^3 of air per second.

[7] Based on the original NCAR design, with some refinement and a new data acquisition system, MASP S/N 3 was built for NASDA by Aerosys Engineering, Boulder, CO. Alignment of the optical components of the MASP was checked just before BIBLE A and found to be unchanged from earlier tests. After BIBLE A the Mangin mirror deteriorated, apparently from moisture damage, and it was replaced before BIBLE B. Very little change in optical alignment was required, and subsequent checks suggest that it is stable both over time and with changes in operating conditions such as temperature. Calibration of the instrument uses the measured signal from presized polystyrene latex (PSL) beads to scale calculations of Mie scatter, collection in the Mangin mirror, and transmission through the optics. Throughout both campaigns, regular tests using PSL beads with diameters of 505 ± 10, 653 ± 12, and 806 ± 11 nm gave consistent results. Variation in beam intensity across the sampling volume contributes around 15% to the uncertainty in number density determination. It also spreads the range in signal from the nearly monodisperse calibration aerosols to give a coefficient of variation (CV) of about 15% for diameters of individual particles. Uncertainties extrapolated to supermicron aerosol are greater, and in addition, for larger particles, data quality was compromised by a problem with signal digitization in MASP S/N 3.

[8] The scattering cross section for particles detected in a MASP varies by five orders of magnitude through the size range. Within the instrument electronics, three separate levels of amplification are integrated and digitized, and the highest gain signal which is not saturated is passed to the data system. Rapid switching between the analog integrals of differently amplified signals for each of the four detectors enables them to be sequentially digitized by a single 12-bit analog-to-digital converter. Unfortunately MASP S/N 3 as used in this study seems to have a problem in synchronization, so that the three stage pipeline of 4-bit conversions is interrupted, degrading data precision to 8- or 4-bit accuracy for the lower gain channels used for larger particles. The data loss is not apparent for a small sample of particles or for the small PSL spheres used in calibration but instead from unphysical patterns in the distribution, for a large number of particles, of digital data transmitted from the MASP to the in-board data acquisition system. The data for each particle are divided by its measured transit time to find the average scattered light from each particle as a measure of its size. This calculation has the effect of smoothing anomalies in the distribution of the digital data, but the precision remains degraded.

[9] In this paper we do not present derived size distributions but only moments of the distribution: particle number, surface area, and volume. The first of these is very sensitive to the lower size bound for detection; and related variation in the sensitive volume. The higher moments are much less sensitive, but their dependence on particle size gives greater weight to the digitizing errors described above, and Poisson uncertainty dominates at the low concentrations of large particles. "Total" scatter as determined by the MASP is a variable power of diameter over the measurement range, but for large particles it is approximately the second power. Thus it is a better measure of surface area than of particle volume or number concentration. Variation in refractive index and sphericity with aerosol composition and hydration adds further uncertainty, as do other factors both external and internal to the MASP. With several sources of error incompletely quantified, we estimate, from internal consistency in the data and intercomparison of MASPs with other instruments [e.g., *Kuhn et al.*, 1998], that surface area concentration at 1 s time resolution is determined to around 25% CV. For number and volume, CV is perhaps 30%.

[10] The CNC and PSAP are rack-mounted within the aircraft, jointly aspirated and vented through the skin of the fuselage. From the forward-facing inlet, 10 cm above the top of the fuselage, stainless steel tubing (5 mm ID) conveys the sample air stream approximately 3 m to the instruments, and also brings it to cabin temperature. A vacuum pump on the outlet maintains approximately 5 lpm flow at low altitude, giving a flow velocity of about 4 m s^{-1} and a residence time (sampling delay) less than 1 s. Reynolds numbers for airflow in the tube fall from 1400 at the surface to below

500 at high altitude, so turbulent losses should be minimal. The external orifice is larger than optimal, giving a subisokinetic entry velocity of around 40 m s^{-1} which can be expected to enhance the supermicron particle count, countered by inertial losses at bends and junctions. These large particles make a negligible contribution to the CN count, but the PSAP data will be less reliable for black carbon in large particles, especially in smoke cloud.

[11] The CNC system is based on a TSI 3760A Condensation Particle Counter which grows particles to detectable size in supersaturated n-butyl alcohol vapor. Particles above 10 nm in diameter are detected by the instrument, but detection efficiency is high only for particles above about 20 nm diameter according to the manufacturer's tests on NaCl particles. Flow rate is controlled by a critical orifice in the instrument, but measured with a mass flowmeter on the CNC outlet to correct the data.

[12] The PSAP, manufactured by Radiance Research of Seattle, Washington, measures optical extinction of light at 565 nm by accumulated absorbing aerosol on a filter through which sample air is aspirated. The change in absorption over the sampling interval is combined with a transfer coefficient specific to the filter type and volumetric flow rate to derive the optical absorption coefficient, *bap*, in units of m^{-1}. Sources of error include airflow, sampling area, and the effect of scattering, as detailed by *Bond et al.* [1999], who concluded also that the manufacturer's calibration overestimates absorption by a factor of 1.22 ± 0.20. We have not tested the accuracy of the internal mass flowmeter of the PSAP, used to calculate sampled volume, but it will anyway be dominated by pressure variation as detailed below. Sampling spot area was consistent.

[13] To calculate the mass concentration of black carbon in sampled air, *bap* is divided by the specific absorption, σ_{ae}. The manufacturer quotes a nominal value of 10 m^2 g^{-1} for this factor, but it has been shown by *Liousse et al.* [1996] to vary by an order of magnitude with particle composition and size distribution, and it should be measured for the site as done for example by *Baumgardner et al.* [2002] in Mexico City, who found $\sigma_{ae} = 7 \pm 0.5$ m^2 g^{-1} for urban air pollution. With no site specific value, we combine the nominal value above with the correction of *Bond et al.* [1999] to give a value:

$$\sigma_{ae} = 8.2 \text{ m}^2\text{g}^{-1}.$$

[14] In stable operating conditions the PSAP sensitivity to changes in filter absorption gives a precision of 10^{-6} m^{-1}, or 0.1 μg m^{-3} of soot, for a 1-min sampling interval. In the polluted conditions in the aircraft hangars at Nagoya and Bandung, 20 min of operation darkened the filter to the extent that light transmission fell below working level. In flight the instrument is subject to variation in filter transmission from changing pressure on the aspirated filter, and moisture in the air stream can markedly change transmission. The result of these effects is frequent "detection" of negative soot, corresponding to increased filter transmission, and corresponding false positive detection on descent or as the filter dries. The data presented here are derived from reanalysis of the primary transmission data using a moving average to correct the times for determination, and to correct as far as possible for the other sources of error. Our calculation of *bap* agrees with the manufacturer's for hangar data, and gives much better results in flight.

[15] In the clean conditions throughout BIBLE A, and in the upper troposphere during BIBLE B, there was insufficient soot to make detection reliable. However many BIBLE B flights showed a large net change in filter transmissivity over the flight and, as shown below, horizontal profiles in dry air yielded soot measurements that correlate well with other tracers of burning.

3. Results

[16] Throughout BIBLE A, and in the ferry flights for BIBLE B, the aircraft frequently flew through cloud. These times are immediately recognizable in the MASP data as particle surface area and volume increases by two or three orders of magnitude. Relative humidity (RH) data for the aircraft also show an increase. Trapped moisture in the inlet for the CR-2 (Buck Research) water vapor sensor, especially from condensation during descent, seems to have resulted in overestimation of humidity at times, but the measurements below 90% RH do not appear to be affected. Selecting cloud-free data by the criterion that RH < 90% from 10 s averages for all flights south of 15°N latitude in BIBLE A gives vertical profiles of aerosol surface area concentration as shown in Figure 1a. In analogy to the presentation of gas concentrations as mixing ratios, the aerosol data are scaled by air density to clarify the relevance of vertical mixing. Above the ubiquitous haze in the boundary layer of the Indonesian islands, the free troposphere was generally clean and free of obvious anthropogenic influence. The pattern of diminishing aerosol surface area with altitude to around 5 km altitude is similar to that seen by *Kristament et al.* [1993] for example, and consistent with theories of aerosol generation and removal for the tropical western Pacific. The mixture of ascents, descents, and (predominantly) horizontal flights would give uneven weighting in a contour plot of these data, so instead the scatterplots are overlaid with lines connecting deciles for 1 km layers to aid comparison with subsequent plots.

[17] Figure 1b shows the corresponding CN concentration data scaled by air density to represent the CN mixing ratio. These data typically show a minimum of around 500 cm^{-3} (STP) at an altitude of 4 km, and increase above that to peak at around 10 km altitude. At this height median CN mixing ratio is greater than in the boundary layer, and the higher deciles much greater, indicating new particle formation in the upper troposphere from precursor gases rather than convection of surface-derived aerosols. The highest CN concentrations occur in the vicinity of cloud, and plots of CN against aerosol surface area at these altitudes (not shown) exhibit some anticorrelation, as new particle formation is favored when aerosol surface area is low [*Clarke et al.*, 1998]. The tropical troposphere may be a major source of nuclei for background aerosol formation in the stratosphere, where nucleation is inhibited [*Brock et al.*, 1995], but this topic belongs in the context of later BIBLE C data; here we note simply the typical range of aerosol measurements in the absence of any tracers of biomass burning during the La Niña conditions of BIBLE A.

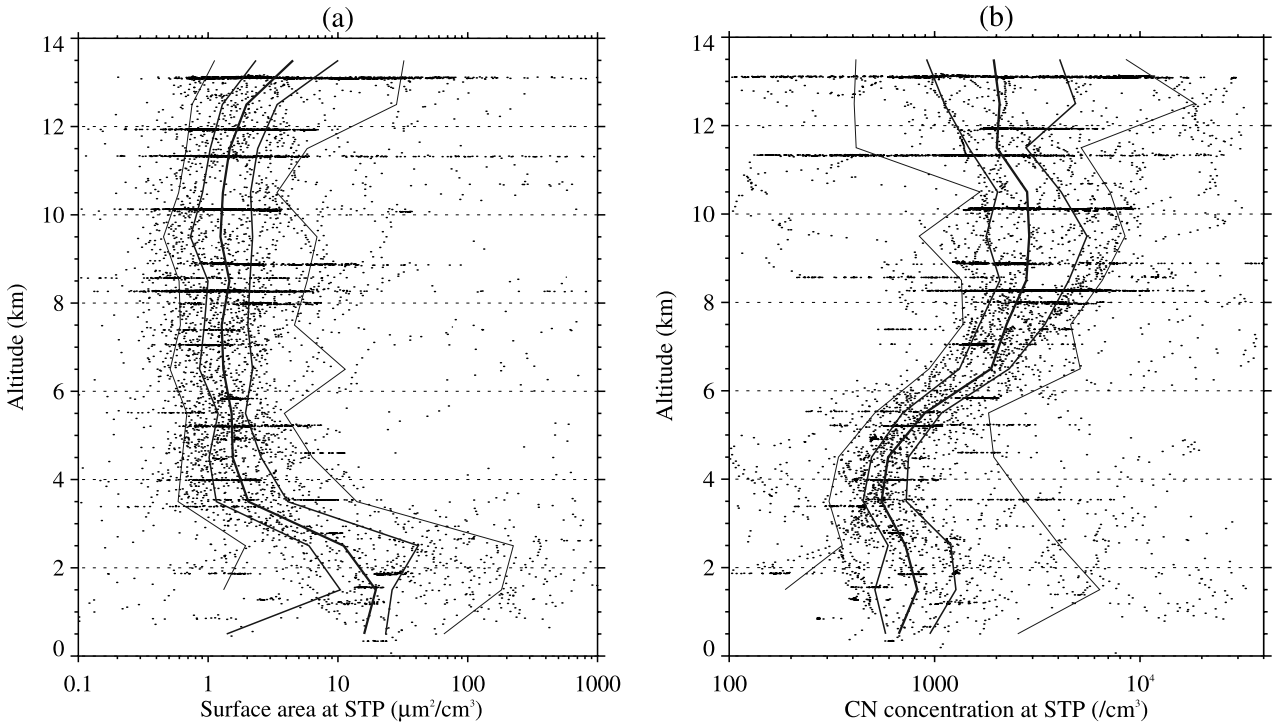

Figure 1. Altitude profiles of mixing ratio for aerosol surface area and condensation nuclei in cloud-free conditions from all BIBLE A flights south of 15°N (12 flights, 10 days, 46 hours sampling), overlaid with percentiles at 10, 30, 50, 70 and 90 for each 1-km layer.

[18] Conditions for BIBLE B over northern Australia at the end of the dry season were very different. The aircraft did not fly through cloud above 4 km altitude (Figure 2a), and in the absence of high level cloud total surface area of submicrometer aerosol was often enhanced. There was less evidence of recent particle formation, with upper deciles of CN concentration much reduced and a somewhat lesser median than at corresponding altitudes in BIBLE A (Figure 2b).

[19] BIBLE B measured high concentrations of biomass-burning products on many flights. At these times CN and coarse aerosol concentrations were markedly enhanced, and correlated with other tracers. The aerosol and CN were mostly confined to altitudes below 4 km, corresponding to the visible distribution of smoke plumes. Very high concentrations of soot were detected during flights at these altitudes.

4. Black Carbon Mass

[20] Figure 3 shows MASP, CN, and PSAP data from flight 7 over Arnhem Land at around 1730 m altitude on 4 September 1999. The soot concentration between 05:10 and 05:25 UT is around 10 μg m^{-3} while the total aerosol volume detected by the MASP is around 20 μm^3 cm^{-3}. Particle sizing for the MASP has assumed sulfate parameters for refractive index $n = 1.45$, and a corresponding mass density of 1.6 g cm^{-3} gives the top line shown in Figure 3a. This would suggest that soot represents about one third of the aerosol by mass detected by the MASP. Such a high proportion of soot requires reconsideration of the optical size determination. For comparison Figure 3a also shows a calibration assuming spheres with the characteristics of black carbon: $n = 2.06 - 0.61i$, and density of 2.0 g cm^{-3}. Absorption within large soot particles causes them to scatter less light into the MASP detectors than sulfate particles of the same size, so that calibration for the latter would cause black carbon spheres to be undersized. For small particles ($d < \lambda = 0.78$ μm) both the larger real refractive index and the imaginary component increase total scatter [e.g., *Hansen and Travis*, 1974], with the result that small spheres are oversized in the MASP for sulfate calibration. In the present case, most of the soot particles are in the latter category, so the calibration based on parameters for black carbon reduces the derived mass. Soot particles are not typically spherical but instead are loose aggregates or branched chains of small ($d \sim 20$ nm) spheres [*Pueschel et al.*, 1992]. We are unable to provide a calibration of the MASP for such particles, but they may be expected to scatter more light than a sphere of equal mass, leading to even smaller calculated mass than shown for soot in Figure 3. On the other hand, soot particles may be coated by liquid, including water from combustion, ambient sulfate, and less volatile organics, making them spherical and reducing the real and imaginary parts of the refractive index. For this reason we may expect the total soot mass detected by the MASP to fall between the curves of Figure 3a.

[21] Total aerosol mass will be greater than that detected by the MASP, which misses particles below about 0.3 μm in diameter. The CN counter detects all particles of diameter greater than about 20 nm, and Figure 3b compares the total counts for the CNC and MASP over the same interval, but note the difference in scale. If all of the particles missed by the MASP were immediately below the size threshold then the true particulate mass would be greater by a factor

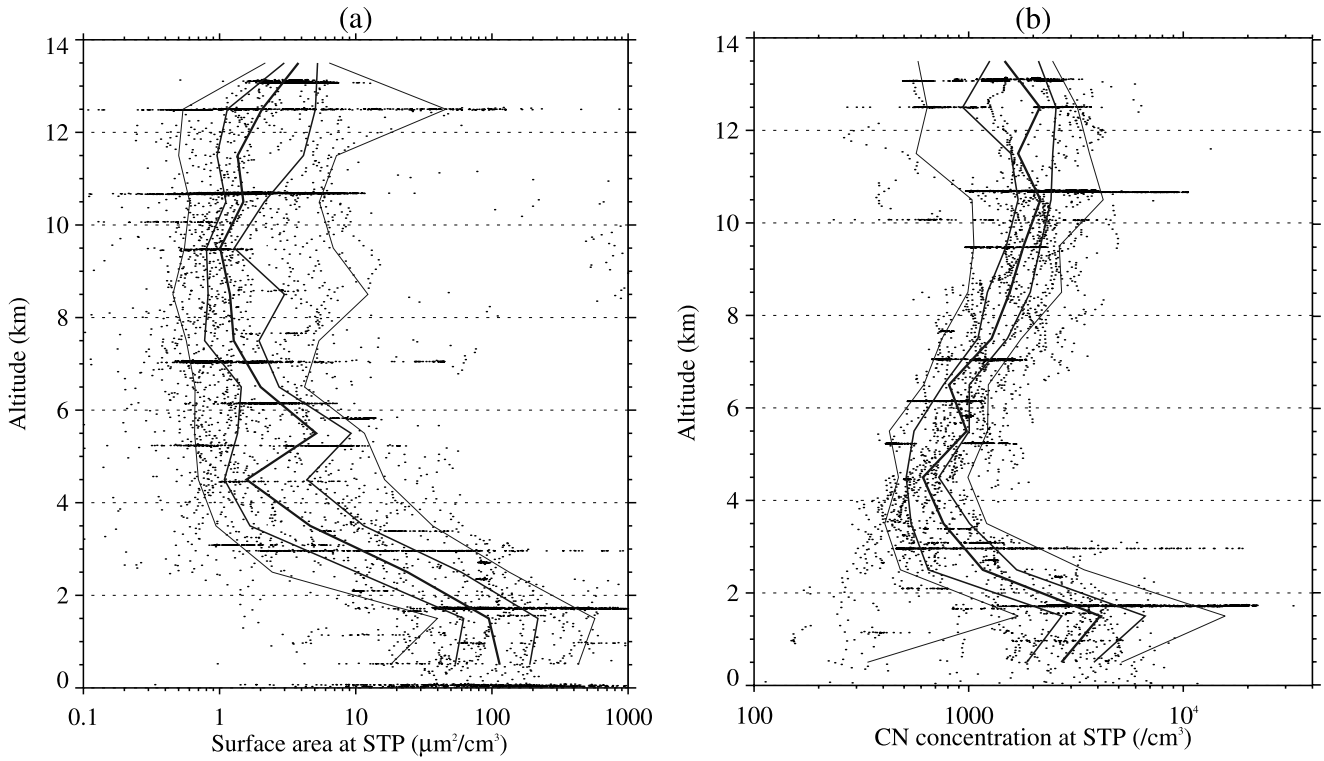

Figure 2. Altitude profiles of mixing ratio for aerosol surface area and condensation nuclei in cloud-free conditions from all BIBLE B flights south of 15°N (10 flights, 6 days, 36 hours sampling). Percentiles at 10, 30, 50, 70 and 90 for each 1-km altitude step are overlaid.

of 10 or more, but such a narrow size distribution is very improbable. Instead we may assume a lognormal size distribution for a small particle mode, and then the ratio of CN-detected particles N_C to MASP-detected particles N_M gives the missing particle volume $V_{S,\delta}$ according to the equations:

$$t = \mathrm{erf}^{-1}\left(\frac{N_C - N_M}{N_C}\right)$$

$$V_{s,\delta}(t) = \frac{\pi}{6} N_C\, \delta^3 \exp\left(\frac{9}{2}s^2 - 3st\right)\mathrm{erf}(t - 3s)$$

where erf( ) is the N(0,1) error function, $s = \ln \sigma_g$ is the lognormal standard deviation, and δ is the size cutoff for the MASP.

[22] Lognormal size distributions for submicron aerosols typically have $s \sim 0.6$–0.7 [*D'Almeida et al.*, 1991], but we do not have a soot-specific value. *Blake and Kato* [1995] sized soot particles by electron microscopy, and though the authors do not quote variance or standard deviation, mean radii for samples of 40 have a distribution in the troposphere consistent with all soot particles coming from a single lognormal distribution with $s = 0.8$ (and mean radius = 0.112 μm). Within a region and season lesser variation seems reasonable. For the MASP we assume in general that $\delta = 0.3$ μm, but $\delta = 0.4$ μm is also considered below. The (probable) presence of a second larger particle mode accounting for much of the particle mass has almost no effect on the calculation as N_C is dominated by the small mode.

[23] The ratio of total particle volume to that measured by the MASP,

$$R_{s,\delta} = \left(\frac{V_M + V_{s,\delta}}{V_M}\right),$$

provides a conversion factor from MASP-detected mass to total mass if particle densities are the same. For the interval shown in Figure 3 we determine

$$R_{0.6,0.3\mu m} = 2.16 \pm 0.20$$

$$R_{0.6,0.4\mu m} = 2.72 \pm 0.30$$

$$R_{0.7,0.3\mu m} = 1.58 \pm 0.09$$

[24] We conclude that approximately half the total particle mass is detected by the MASP in the smoke plumes, and therefore that particulate black carbon is about one quarter of the total. This proportion is higher than observed by *Gras et al.* [1999], who indicated that soot made up about 1/9 of the aerosol mass determined from nephelometer measurements near Katherine, NT, which is in a source region for plumes sampled in BIBLE B. A lower value of σ_{ae} than 8.2 m^2 g^{-1}.would further increase the derived black carbon as a proportion of aerosol mass. Similarly MASP recalibration for absorbing particles suggests a higher proportion of soot, but the consequences of large asphericity are unknown. Even for spherical particles of known refractive index, a 30% CV gives 95% confidence limits with nearly a factor of 3 from

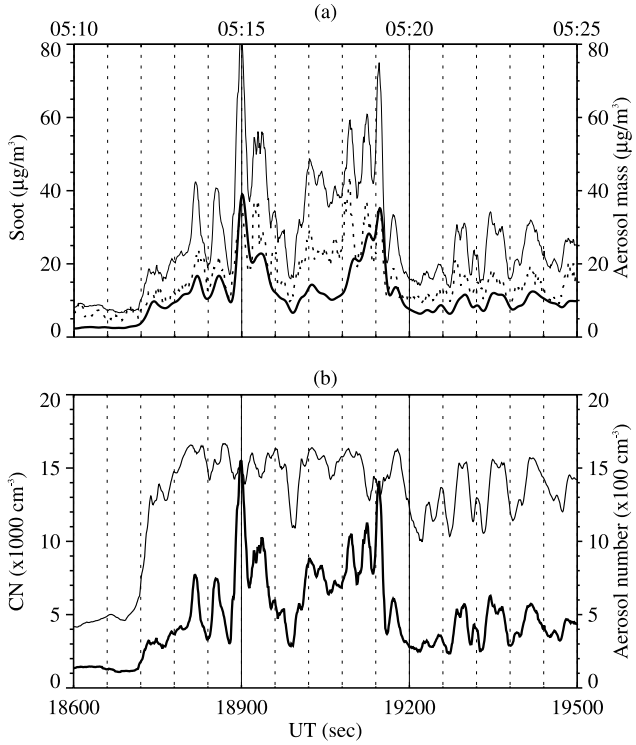

Figure 3. Particle data for BIBLE B flight 7 at 1700 m altitude over Arnhem Land on 4 September 1999. Local time is UT + 9:30. (a) Black carbon calculated as soot mass (thick line) from PSAP data, and total aerosol mass for particle diameter $d > 0.3$ μm, on the same scale, based on sulfate (thin line) and soot (dotted line) calibrations of MASP data. (b) Condensation nuclei (thin line) and aerosol number concentration, $d > 0.3$ μm (thick line). Note that the scales differ by a factor of 10.

lowest to highest, so we cannot conclude that our results are inconsistent with those of *Gras et al.* [1999].

5. Emission Ratios

[25] At times of high soot concentration, simultaneous increases in carbon monoxide, carbon dioxide and hydrocarbons were observed during BIBLE B. Figure 4 shows plots of CO and CO_2 mixing ratios versus soot concentration at standard temperature and pressure (STP), analogous to a mixing ratio. Both plots show mostly compact distribution for the times when these species were strongly enhanced, which was predominantly on flights 6 and 7 (2 and 4 September 1999) within 500 km east and south of Darwin. Many other flights detected similar products as they ascended or descended through the 0–3 km layer, but only flights 6 and 7 sampled them extensively in level flight, when there was no ambiguity due to pressure changes in PSAP measurements. Some other data, especially those for relative humidity, were affected by condensation in the inlet line during rapid descents.

[26] In level flight at just below 3000 m altitude on flight 7, above a region of burning due south of Darwin, the PSAP measured the highest concentration of black carbon in the BIBLE data series. The data form a narrow peak, but these points were not correspondingly extreme in CO or CO_2 mixing ratio. From the MASP data, particulate volume is more than 20 times greater than for the period in Figure 3, and relative humidity (RH) reaches 100%, showing that the

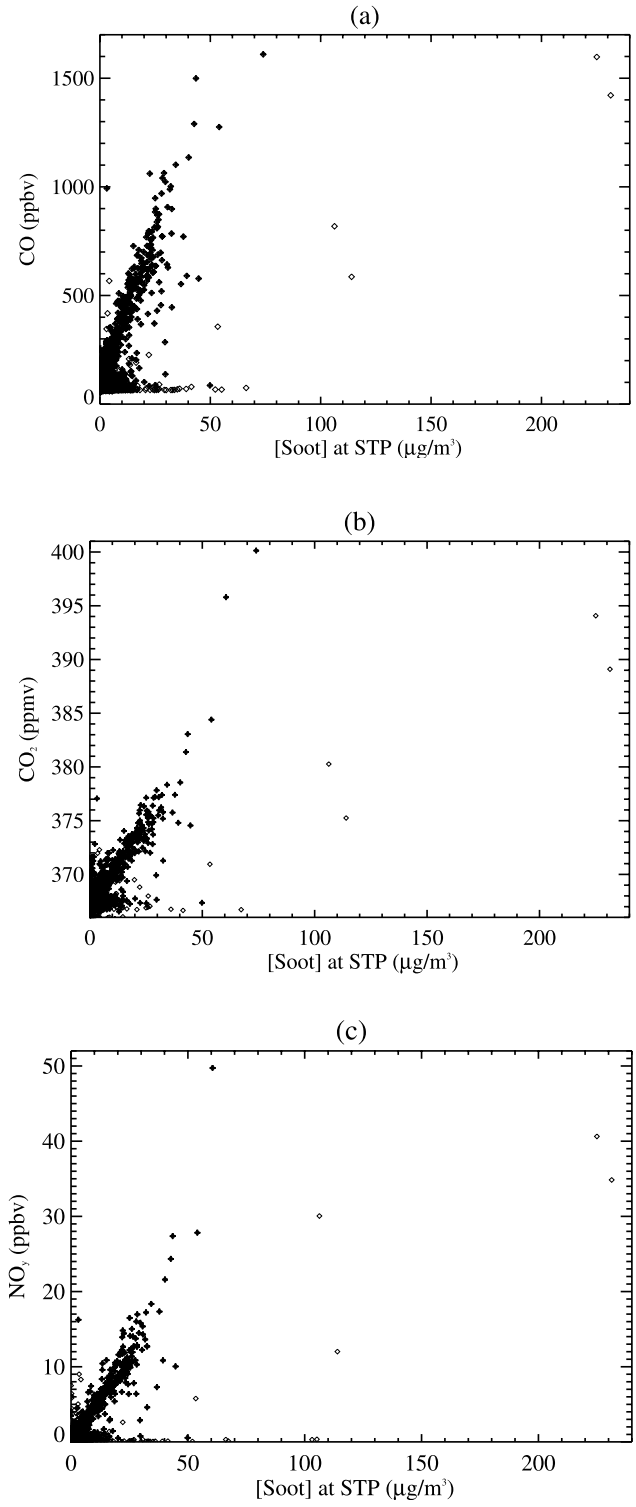

Figure 4. Mixing ratios of (a) carbon monoxide, (b) carbon dioxide, and (c) reactive nitrogen versus soot concentration at STP. Open symbols, for RH > 90%, designate data from within smoke cloud.

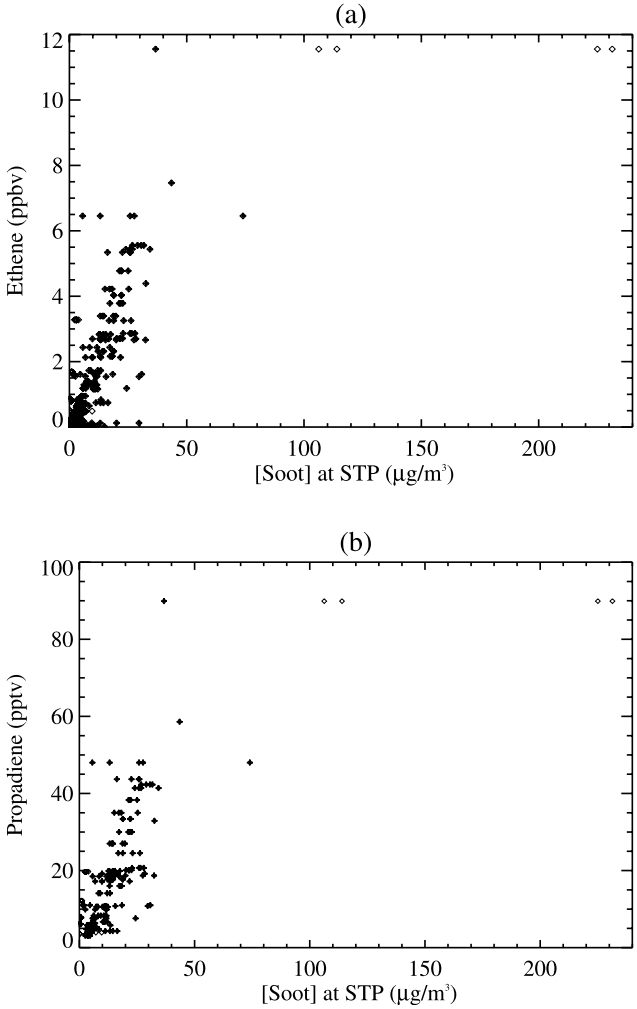

Figure 5. Mixing ratios of (a) ethene and (b) propadiene versus soot concentration at STP. Open symbols denote RH > 90%.

aircraft was flying through smoke cloud. To clarify this distinction, the data for RH > 90% are shown with open symbols in Figure 4.

[27] With whole-air sampling and subsequent analysis by gas chromatography, numerous hydrocarbons are measured on the BIBLE flights [*Shirai et al.*, 2002]. In Figure 5 the soot concentration at STP is compared with mixing ratios for two of them. Because it takes from tens of seconds to several minutes (at high altitude) to collect each air sample, the hydrocarbon data are treated here as averages over the full sampling period, so that four or more soot values on the abscissa correspond to the same ordinate. The peak in measured soot concentration, at 231 $\mu g\ m^{-3}$ for 10 second average, coincides with an air sample in which concentrations of most hydrocarbons were the highest measured in the airborne samples and, as they did for the oxides of carbon, these points fall outside the distribution of the other data. Soot formation ratio in biomass combustion is known to depend on the oxidizing conditions, as determined from the ratio of excess CO to excess CO_2, $\Delta CO/\Delta CO_2$. For the BIBLE B flights 6 and 7 in the boundary layer over Arnhem Land and the vicinity of Darwin, *Shirai et al.* [2002] calculate $\Delta CO/\Delta CO_2 = 0.086 \pm 0.002$ as the slope of a plot of CO versus CO_2 for those times when a canister sample was taken. For the full data set over the same period the CO versus CO_2 data fall in a range $0.06 < \Delta CO/\Delta CO_2 < 0.09$. In particular, the samples with the highest concentrations of soot and hydrocarbons have $\Delta CO/\Delta CO_2 = 0.060$. It is difficult to say from the one brief episode whether these points represent different chemistry in the fires and plume, or the effect of smoke cloud droplets on measurement, especially of soot. Sampling efficiency of the PSAP inlet system for large particles is doubtful, as noted earlier, and for the following we treat these data separately.

[28] As described above, light attenuation in the PSAP is divided by specific absorption to give effective mass of black carbon, consisting of elemental carbon and organic compounds which are strongly light-absorbing. In combustion residues from savanna grass, *Kuhlbusch and Crutzen* [1996] found H/C molar ratios in the range 0.13 to 0.30, and their data suggest that this range should be representative for our measurements. Thus carbon atoms contribute almost all of the mass in black carbon mass. We calculate equivalent molar mixing ratio for atomic carbon in soot C_s on this basis (mol. wt. BC $\sim$ 12.2 g mol^{-1}), and derive emission ratios for C_s by regression for a series of plots like those of Figures 4 and 5. The longer collection times for canister samples and smaller uncertainties in all of the gas phase measurements make them the preferred choice as independent variable in each regression. Results are shown in Table 1 for the subset of data where soot and CO or CO_2 are enhanced and RH < 90%. The uncertainties shown are the standard errors of the regression coefficients; they provide a measure of how tightly an assumed constant emission ratio

Table 1. Emission Ratios for Soot Carbon (C_s) Relative to Gaseous Products of Biomass Burning

	Cloud Free			Smoke Cloud		
Gas Species G	$\Delta C_S/\Delta G$	r^2	N	$\Delta C_S/\Delta G$	r^2	N
CO	0.0620 ± 0.0012	0.877	705	0.308 ± 0.012	0.947	79
CO_2	0.00487 ± 0.00010	0.863	830	0.01720 ± 0.00053	0.950	115
NOy	2.985 ± 0.062	0.861	822	10.28 ± 0.39	0.931	109
CH_4	1.016 ± 0.072	0.635	299	2.66 ± 0.53	0.610	45
Ethane	19.7 ± 1.0	0.764	299	73.4 ± 4.5	0.924	47
Ethene	7.89 ± 0.37	0.791	273	27.4 ± 2.2	0.914	34
Ethyne	18.6 ± 0.9	0.769	299	71.2 ± 6.1	0.869	47
Propene	31.3 ± 1.7	0.753	255	120 ± 9	0.929	31
Propane	96.3 ± 4.6	0.770	299	382 ± 23	0.926	47
Propadiene	946 ± 72	0.719	162			
1-Butene	206 ± 16	0.716	156			
Benzene	65.6 ± 3.1	0.778	299	259 ± 19	0.899	47

(change ΔC_S in C_s associated with change ΔG in the concentration of gas G) is constrained by these data. They do not quantify how representative the data may be, and they are subject to any bias in the measurements, especially in the choice of σ_{ae}.

[29] Emission ratios for the data in cloud (RH > 90%) are included in the table for completeness, but the smaller sample and uncertainty about other factors make these results less likely to be representative. Despite the high correlation coefficients they should be treated with caution.

[30] At about 0.5% of carbon dioxide emissions and 6% of carbon monoxide by molar ratio, black carbon in airborne soot represents a minimal part of the carbon budget in Australian savanna fires. On the other hand soot production is substantial compared with many reactive species, being comparable to that of methane and about 3 times NO_y production in these fires. The importance of airborne soot for trapping short-wave radiation, and its possible role as a surface for heterogeneous chemistry, make this production especially significant.

[31] *Kuhlbusch and Crutzen* [1996, Figure 16.4] summarized published data on ratios of black carbon in smoke and in residues relative to CO_2 emissions for different types of combustion and fuel. Most values for $\Delta C_S/\Delta CO_2$ were in the range 0.15–0.25%, but the largest was 0.8%. Our emission ratio of $\Delta C_S/\Delta CO_2 = 0.49 \pm 0.01\%$ for the atmospheric boundary layer over northern Australian savanna fires is within the range for this ratio close to the combustion source.

6. Conclusions

[32] From the CN, aerosol, and black carbon instruments on the Gulfstream-II aircraft used in the BIBLE campaigns we have estimated that the soot fraction in aerosol from northern Australian savanna burning may be up to one quarter of total aerosol mass at low relative humidity. Soot production expressed as elemental carbon is about 0.5% of carbon dioxide and 6% of carbon monoxide from the same fires. It is comparable to methane production, and greater than that of other hydrocarbons. The production ratios differed in one region of very high tracer concentrations where the measurements were made within cloud. The differences may be a measurement or sampling artifact, as the ratios given above were consistent over a region hundreds of kilometers in extent and containing a large number of fires of varying intensity and combustible material. The ratios given here should be useful in estimating radiative effects of regional biomass burning and as input to models of combustion aerosols and heterogeneous chemistry.

[33] **Acknowledgments.** This work was supported by NASDA under contract to NIWA.

References

Ackerman, A. S., O. B. Toon, D. E. Stevens, A. J. Heymsfield, V. Ramanathan, and E. J. Welton, Reduction of tropical cloudiness by soot, *Science*, *288*, 1042–1047, 2000.

Baumgardner, D., J. S. Dye, B. Gandrud, D. Rogers, K. Weaver, R. G. Knollenberg, R. Newton, and R. Gallant, The multiangle aerosol spectrometer probe: A new instrument for airborne particle research, paper presented at Ninth Symposium on Meteorological Observations and Instrumentation, Am. Meteorol. Soc., Charlotte, N. C., 1995.

Baumgardner, D., G. Raga, O. Peralta, I. Rosas, T. Castro, T. Kuhlbusch, A. John, and A. Petzold, Diagnosing black carbon trends in large urban areas using carbon monoxide measurements, *J. Geophys. Res.*, *107*(D21), 8342, doi:10.1029/2001JD000626, 2002.

Blake, D. F., and K. Kato, Latitudinal distribution of black carbon soot in the upper troposphere and lower stratosphere, *J. Geophys. Res.*, *100*, 7195–7202, 1995.

Bond, T. C., T. L. Anderson, and D. Campbell, Calibration and intercomparison of filter-based measurements of visible light absorption by aerosols, *Aerosol Sci. Technol.*, *30*, 582–600, 1999.

Brock, C. A., P. Hamill, J. C. Wilson, H. H. Jonsson, and K. R. Chan, Particle formation in the upper tropical troposphere: A source of nuclei for the stratospheric aerosol, *Science*, *270*, 1650–1653, 1995.

Chughtai, A. R., M. E. Brooks, and D. M. Smith, Hydration of black carbon, *J. Geophys. Res.*, *101*, 19,505–19,514, 1996.

Clarke, A. D., et al., Particle nucleation in the tropical boundary layer and its coupling to marine sulfur sources, *Science*, *282*, 89–92, 1998.

Cooke, W. F., and J. J. N. Wilson, A global black carbon model, *J. Geophys. Res.*, *101*, 19,395–19,409, 1996.

D'Almeida, G. A., P. Koepke, and E. P. Shettle, *Atmospheric Aerosols: Global Climatology and Radiative Characteristics*, 561 pp., A. Deepak, Hampton, Va., 1991.

Gras, J. L., J. B. Jensen, K. Okada, M. Ikegami, Y. Zaizen, and Y. Makino, Some optical properties of smoke aerosol in Indonesia and tropical Australia, *Geophys. Res. Lett.*, *26*, 1393–1396, 1999.

Hansen, J. E., and L. D. Travis, Light scattering in planetary atmospheres, *Space Sci. Rev.*, *16*, 527–610, 1974.

Kondo, Y., et al., Effects of biomass burning, lightning, and convection on O_3, CO, and NO_y over the tropical Pacific and Australia in August–October 1998 and 1999, *J. Geophys. Res.*, *107*, doi:10.1029/2001JD000820, in press, 2002.

Kristament, I. S., J. B. Liley, and M. J. Harvey, Aerosol variability in the vertical in the southwest Pacific, *J. Geophys. Res.*, *98*, 7129–7139, 1993.

Kuhlbusch, T. A. J., and P. J. Crutzen, Black carbon, the global carbon cycle, and atmospheric carbon dioxide, in *Biomass Burning and Global Change*, vol. 1, edited by J. S. Levine, pp. 160–169, MIT Press, Cambridge, Mass., 1996.

Kuhn, M., A. Petzold, D. Baumgardner, and R. P. Schröder, Particle composition of a young condensation trail and of upper tropospheric aerosol, *Geophys. Res. Lett.*, *25*, 2679–2682, 1998.

Liousse, C., J. E. Penner, C. Chuang, J. J. Walton, H. Eddleman, and H. Cachier, A global three-dimensional model study of carbonaceous aerosols, *J. Geophys. Res.*, *101*, 19,411–19,432, 1996.

Novakov, T., and J. E. Penner, Large contribution of organic aerosols to cloud-condensation-nuclei concentrations, *Nature*, *365*, 823, 1993.

Pósfai, M., J. R. Anderson, P. R. Buseck, and H. Sievering, Soot and sulfate aerosol particles in the remote marine troposphere, *J. Geophys. Res.*, *104*, 21,685–21,693, 1999.

Pueschel, R. F., D. F. Blake, K. G. Snetsinger, A. D. A. Hansen, S. Verma, and K. Kato, Black carbon (soot) aerosol in the lower stratosphere and upper troposphere, *Geophys. Res. Lett.*, *19*, 1659–1662, 1992.

Rawlins, W. T., S. G. Kang, D. M. Sonnenfroh, K. L. Carleton, and B. E. Wyslouzil, Activation of carbon aerosol by deposition of sulfuric acid, in *Biomass Burning and Global Change*, vol. 1, edited by J. S. Levine, pp. 540–544, MIT Press, Cambridge, Mass., 1996.

Shirai, T., et al., Emission estimates of selected volatile organic compounds from tropical savanna burning in northern Australia, *J. Geophys. Res.*, *107*, doi:10.1029/2001JD000841, in press, 2002.

D. Baumgardner, Centro de Ciencias de la Atmosfera, Universidad Nacional Autonoma de Mexico, Circuito Exterior s/n, Ciudad Universitaria, 04510 Mexico City, Mexico. (darrel@servidor.unam.mx)

D. R. Blake, Department of Chemistry, University of California, Irvine, CA 92697-2025, USA. (dblake@orion.oac.uci.edu)

S. Kawakami, T. Ogawa, and T. Shirai, Earth Observation Research Center, National Space Development Agency of Japan, 1-8-10 Harumi, Chuou-ku, Tokyo 106-0032, Japan. (kawakami@eorc.nasda.go.jp; t_ogawa@eorc.nasda.go.jp)

K. Kita, N. Takegawa, and Y. Kondo, Research Center for Advanced Science and Technology, University of Tokyo, 4-6-1 Komaba, Meguro-ku, Tokyo 153-8904, Japan. (kita@atmos.rcast.u-tokyo.ac.jp; takegawa@atmos.rcast.u-tokyo.ac.jp; kondo@atmos.rcast.u-tokyo.ac.jp)

M. Koike, Department of Earth and Planetary Science, Graduate School of Science, University of Tokyo, 7-3-1 Hongo, Bunkyo-ku, Tokyo 113-0033, Japan.

J. B. Liley, NIWA Lauder, Private Bag 50061, Omakau, Central Otago, New Zealand. (b.liley@niwa.cri.nz)

T. Machida, National Institute of Environmental Studies, 16-2 Onogawa, Tsukuba, Ibaraki 305-8506, Japan. (tmachida@nies.go.jp)